Heliyon 10 (2024) e39126

Contents lists available at ScienceDirect

Heliyon

journal homepage: www.cell.com/heliyon

Research article

Lactobacillus rhamnosus ameliorates experimental autoimmune neuritis via modulation of gut microbiota and metabolites

Peng Shi [a], Yu Li [a], Hui Yang [a], Qiang Li [a], Qianqian Li [a], Ming Ye [a], Di Nian [b,*]

[a] Department of Neurology, First Affiliated Hospital of Bengbu Medical College, Bengbu 233004, China
[b] Department of Medical Examination, Bengbu Medical College, Bengbu 233030, China

ARTICLE INFO

Keywords:
EAN
Lactobacillus rhamnosus GG
Gut microbiota
Guillain-Barré syndrome

ABSTRACT

Background: Guillain-Barre syndrome (GBS), an autoimmune disease of the peripheral nervous system, is hallmarked by demyelination and immune cellular infiltration. Experimental autoimmune neuritis (EAN), considered a GBS prototype model, has been studied for its potential therapeutic benefits from lactobacilli. This study evaluated the protective role of Lactobacillus *rhamnosus* GG (GG) for treatment in EAN. T cell ratio, inflammation factors, sciatic nerve pathology, intestinal permeability, and gut inflammation were assessed on day 19 post-immunization to evaluate GG's effect on EAN. Fecal metabolomics and 16s rRNA microbiome analysis were conducted to elucidate its mechanism.

Results: GG dynamically balanced $CD4^+/CD8^+$T cell ratio, reduced serum IL-1β and TNF-α expression, improved sciatic nerve demyelination and inflammation, and enhanced neurological scores during peak disease period. Intestinal mucosal damage was evident in EAN rats, with downregulated Occludin and ZO-1 and upregulated IL-1β, TNF-α, and Reg3γ. GG treatment restored intestinal mucosal integrity, upregulated Occludin and ZO-1, and downregulated IL-1, TNF-α, and Reg3γ. GG partially rectified the gut microbiota and metabolite imbalance in EAN rats.

Conclusion: GG mitigates EAN through immune response modulation and inflammation reduction via the gut microbiota and metabolites.

1. Introduction

Guillain-Barré Syndrome (GBS), an immune disorder of the peripheral nervous system (PNS), features acute flaccid paralysis and autonomic dysfunction [1]. It has a worldwide annual incidence rate of between 0.81 and 1.89/100,000 people, escalating exponentially with age in certain Western countries [2], presenting severe potential for fatality or disability among 3–10 % and 20 % of patients respectively [3]. Intravenous immunoglobulin (or plasma exchange) is currently the optimal treatment for GBS [4]. The most common form of GBS clinically is Acute Inflammatory Demyelinating Polyneuropathy (AIDP) [5]. The experimental autoimmune neuritis (EAN) animal model, a classic representation of AIDP, exhibits T cell and macrophage infiltration into PNS, inflammatory demyelination, and axonal damage in sciatic nerves [5], mirroring GBS's pathological and immunological characteristics.

GBS, a prevalent and severe PNS disease, primarily results from preceding *Campylobacter jejuni* infection or other immune stimuli triggering autoimmune responses leading to PNS damage. In mouse models, *C. jejuni* preinfection elevates GBS risk, but postinfection

* Corresponding author.
E-mail address: Niandi1234@126.com (D. Nian).

https://doi.org/10.1016/j.heliyon.2024.e39126
Received 16 June 2024; Received in revised form 23 September 2024; Accepted 8 October 2024
Available online 9 October 2024

lactobacillus therapy mitigates inflammation and autoimmune disease severity [6]. Antiganglioside autoantibodies significantly increase following *C. jejuni* infection, linked to dominant bacterial communities including Bacteroidetes and Firmicutes [7]. These findings underscore the role of gut microbiota in GBS development.

Lactobacilli have been associated with autoimmune diseases [8]. *Lactobacillus reuteri* ameliorated EAN by reducing Th17 cells [9]. In systemic lupus erythematosus mice, *Lactobacillus rhamnosus* GG (GG) increased regulatory T cells, reduced proinflammatory cytokines, and alleviated autoimmune diseases [10]. Moreover, lactobacilli exhibit anti-inflammatory effects via decreasing IL-6 and increasing IL-10 levels in the intestine [11]. Some lactobacilli produce protective compounds like short chain fatty acids (SCFAs). SCFAs act as local mediators of bacteria-gut epithelium communication [12,13]. SCFAs stimulate epithelial cells to generate retinoic acid, a vitamin A derivative. Retinoic acid synergizes with TGF-β to promote T cell differentiation towards regulatory T cells and inhibit Th17 cell differentiation [14]. Numerous lactobacilli can reprogram $CD4^{+}$T cells into immunoregulatory T cells, playing crucial roles in immune response regulation and tolerance [15]. These studies suggest that lactobacilli alleviate autoimmune and inflammatory diseases.

Currently, there are no effective treatments for EAN, which is closely related to T cell immune regulation and inflammation in the PNS. Conducting comprehensive literature research and preliminary tests, we identified GG's superior EAN protection. This study delved deeper into the mechanisms of action of GG. We propose that GG may improve EAN progression through restoring immune imbalance and inflammation.

2. Materials and methods

2.1. Bacterial culture

The GG (ATCC53103) strain was inoculated onto MRS solid medium at 37 °C for 24 h. After transferring to MRS liquid medium, the bacteria were grown at 37 °C for another 12 h until stationary phase. Bacteria were centrifuged at 4200 rpm/min for 15 min then resuspended in PBS.

2.2. Establishment of EAN model

Female Lewis rats aged six to eight weeks with a body weight range between 140 and 160 g (n = 24), procured from Beijing Weitonglihua Experimental Animal Technology Co., Ltd., underwent one week's acclimatization at the animal management center. The animals were randomly divided into four groups (n = 6): the control group, the EAN model group, the H-GG group, and the L-GG group. EAN was induced using neurotrophic P0180-199 peptide (300 μg, MCE, USA) emulsified in complete Freund's adjuvant containing *Mycobacterium tuberculosis* H37RA (10 mg/ml). Each rat received 300 μl injected into the sole on day 7, followed by a booster immunization after 7 days. Successful modeling was indicated by tail paralysis, hindlimb weakness, forelimb weakness, gait or posture abnormalities, and reduced activity, weight loss, and depressed mental state. Disease severity was assessed daily using an EAN scoring system: 0-normal; 1-limb damage; 2-no correction; 3-gait or posture abnormality; 4-mild paraplegia; 5-moderate paraplegia; 6-severe paraplegia; 7-tetraplegia; 8-moribund; 9-death. From one week prior to experimentation to post-modeling day 19, both the H-GG and L-GG groups received intragastrically 10^9 CFU and 10^6 CFU in 200 μl saline, while the control and model groups received saline. All animals were euthanized on day 19 post-modeling.

2.3. Excision and fixation of sciatic nerve

The animal subjects were euthanized on day 19 post immunization, ensuring the dissection of their connective and muscular leg tissues to expose the sciatic nerve, then its isolation was achieved by clipping both right and left nerve branches. A total of 1 cm of spinal nerves were collected from both sides, subjected to fixation in a 4 % formaldehyde solution.

2.4. Hematoxylin-eosin staining

Sciatic nerves fixed with a 4 % formaldehyde solution underwent tissue embedding and sectioning. Slice immersed in xylene twice, 5 min each. Followed by respective immersions in 100 %, 95 %, 85 %, 75 %, and 50 % ethanol for 5 min each. Post immersion, washed with sterile PBS thrice (5 min each), then rinsed in distilled water for another 5 min. Hematochrome staining was carried out for 8–10 min, followed by hydrochloric alcohol dipping for 10 s before rinsing with water for 5 min. Later, they were soaked in a saturated lithium carbonate solution for 5 s, rinsed again, dyed with eosin for 25 s, and finally rinsed in ethanol solutions of 95 % and 100 % for 10 s each. After sealing with neutral resin, the sciatic nerve tissue was observed under a microscope.

2.5. Luxol Fast Blue demyelination staining

Sciatic nerve paraffin sections were dewaxed, washed with distilled water, and stained following the instructions of the Luxol Fast Blue kit (Beijing, China). The myelin morphology of the sciatic nerve tissue was examined under a microscope.

2.6. Transmission electron microscopy examination

The sciatic nerve was fixed at room temperature in an electron microscopy fixative solution prior to being sent to servicebio (Wuhang, China) for embedding and ultrathin sectioning. Following staining with uranyl acetate and lead citrate, it was observed under a cryogenic transmission electron microscope (Thermo, MA, USA).

2.7. Flow cytometry analysis of T cell differentiation in tail vein blood

A total of 200 μL of tail vein blood was collected from the animals during the peak disease period (day 19), mixed with 600 μL of red cell lysis buffer (Solarbio, Beijing, China), inverted three times, chilled for 15 min, and centrifuged at 450 g/min for 10 min at 4 °C. The above operation was repeated once and washed with PBS thrice. The Fixable Viability Dye eFluor 506 (Thermo, MA, USA) was diluted to 1:1000 with PBS, and 100 μL of this solution was added to resuspend the cell pellet. This was incubated at 4 °C in the dark for 30 min, centrifuged at 1800 rpm/min for 5 min at room temperature, and the supernatant discarded. Each well was resuspended with 200 μL of 1 % FACS (0.5 g BSA + 50 mL PBS), centrifuged at 1800 rpm/min for 5 min at 4 °C, and the supernatant aspirated. Cells were resuspended in 1 μLCD3, CD4, CD8 antibodies (BD, Beijing, China) or 1 % FACS, incubated at 4 °C in the dark for 30 min, centrifuged at 1800 rpm/min for 5 min at 4 °C, and the supernatant discarded. The cells were resuspended in 500 μLPBS and analyzed using a Cytek flow cytometer (Thermo, USA).

2.8. ELISA

The supernatant was obtained after blood collection in anticoagulant tubes at 4 °C for 30 min with a centrifugation speed of 1000 g/min for 15 min. For tissue samples, a small piece of intestine was minced, homogenized using PBS chilled in an ice bath, then centrifuged at 5000 g/min for 5 min to collect the supernatant. The detection of IL-1β and TNF-α (Thermo, MA, USA) followed the manufacturer's instructions.

2.9. Alcian staining

Colon tissue was fixed in 4 % paraformaldehyde, embedded, and sectioned for Alcian staining (Beijing Biyuntian, China). This procedure was followed by microscopic observation.

2.10. Real-time quantitative PCR

RNA was extracted according to the RNA extraction kit (Takara, Shanghai, China), followed by reverse transcription setup using Takara's PrimeScript™ RT reagent Kit, and reaction conditions of 37 °C for 15 min and 85 °C for 5 s cDNA samples are diluted appropriately before being used in the reaction system consisting of forward Primer 0.4 μL, Reverse Primer 0.4 μL, RNase Free ddH_2O 8.2 μL, SYBR Green qPCR Mix 10 μL, cDNA 1 μL. All added up to 20 μL. The reaction mixture underwent one cycle of 95 °C for 10 min, then 40 cycles of 95 °C for 15 s, 60 °C for 30 s and 72 °C for 45s. Employing the $2^{-\Delta\Delta Ct}$ method, the target gene mRNA transcription level was calculated based on the number of cycles. Primers used included Occludin, CATAGTCTCCCACCATCCTC and ACAAAGAGCTCTCTCGTCTCG; ZO-1, GCTTAAAGCTGGCAGTGTC and AGTTCTGCCCTCAGCTACCA; Reg3γ, GCCTTGAACTTGCAGACAT and AACTGGGAGACGAATCCTT; Gapdh, TTATGGGGTCTGGGATGG and ATGGCTACAGCAACAGGGT.

2.11. 16S ribosomal RNA gene sequencing

Genomic DNA from colonic fecal samples was extracted using SDS method, checked for purity and concentration, amplified by PCR targeting selected regions, and sequenced on Illumina NovaSeq 6000 platform. Raw sequences undergo preprocessing, alignment against reference databases, and calculation of relative abundance of different species per sample. α diversity, β diversity, and Anosim tests were performed.

2.12. Non-targeted metabolomics analysis

Non-targeted metabolomics analysis of gut microbiota involves extracting approximately 2 μL supernatant from colon fecal specimens mixed with a cold methanol/acetonitrile/water solution (2:2:1), sonication at −20 °C for 15 min, centrifugation at 14000 g/min for 20 min at 4 °C, and mass spectrometry analysis (AB Triple TOF 6600, Thermo). Raw data underwents format conversion, data processing, metabolite structure identification, quality control, and reliability testing. Differentially abundant metabolites between groups were identified using PLS-DA model with VIP >1 and $p < 0.05$ considered significant. KEGG pathway analysis was conducted to visualize screening results as heat maps.

2.13. Statistical analysis

Statistical analysis is carried out using GraphPad Prism 9 software. Data were presented as mean ± standard deviation. T test was used for comparison between two groups, ANOVA for multiple groups, and $p < 0.05$ indicates statistical significance.

3. Results

3.1. GG alleviates EAN symptoms

No significant weight differences were noted between treatment groups during disease progression (Fig. 1A). EAN onset in the model group occurred on day 9 post-immunization, peaking at day 19. H-GG and L-GG treatments notably ameliorated disease severity (Fig. 1B), suggesting GG's therapeutic potential. HE staining of sciatic nerves post immunization showed profound infiltrations of inflammatory cells in sciatic nerves post-immunization were observed in the EAN model group, which were mitigated by H-GG and L-GG treatments (Fig. 1C). LFB staining revealed intact myelin sheaths in control rats, while the EAN model group displayed extensive myelin loss. Both H-GG and L-GG treatments mitigated this myelin loss (Fig. 1C). Post-immunization day 19, electron microscopy confirmed normal axon arrangement and regular myelin morphology in control rats. In contrast, the EAN model group exhibited

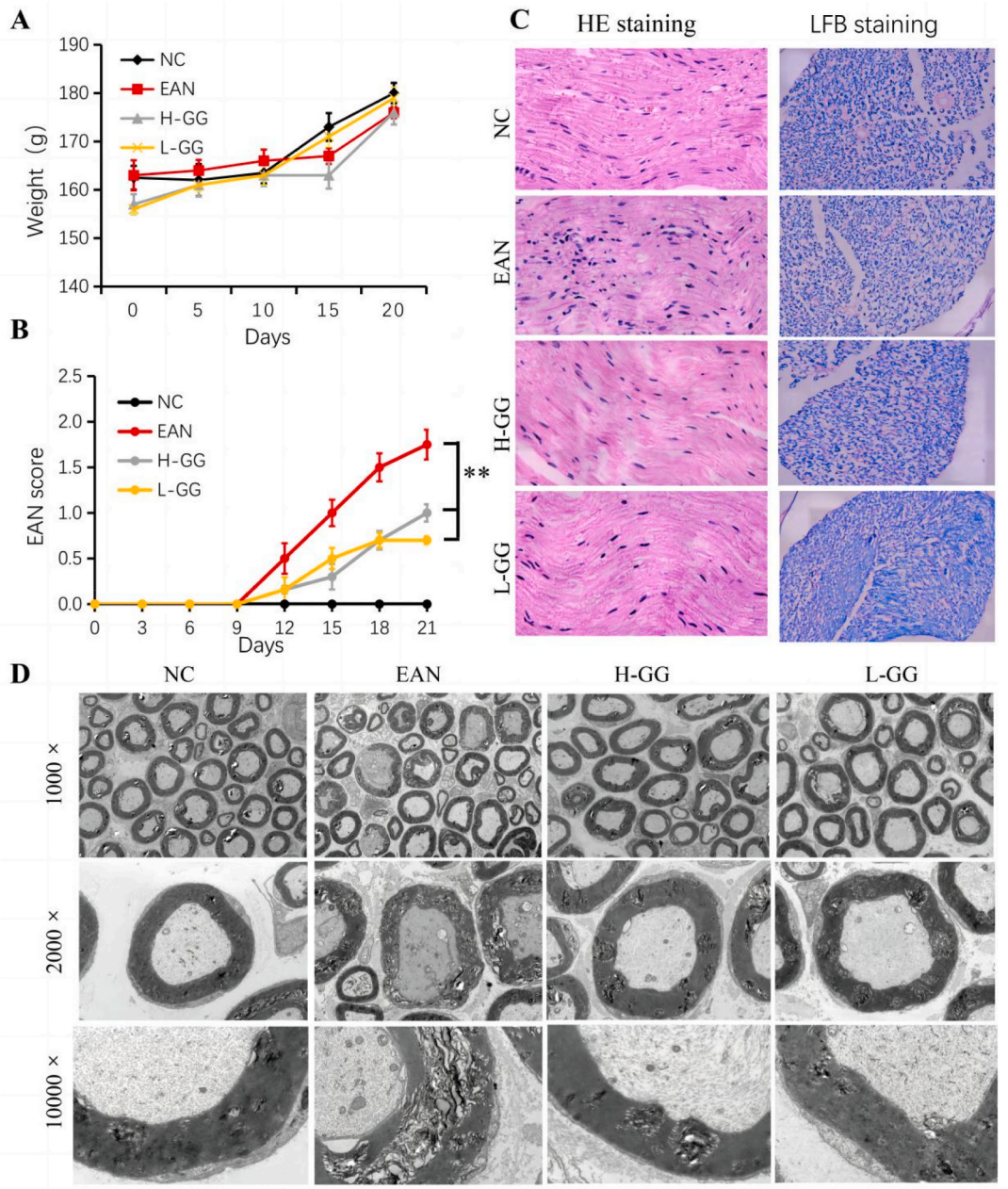

Fig. 1. GG Ameliorates EAN Symptoms (n = 6). A, Animal weights across treatments; B, Behavioral scores during EAN development; C, Sciatic nerve HE and LFB stains; D, Sciatic nerve TEM observations (1000x, 2000x, 10000x). (**$p < 0.01$).

disrupted axons and loose fiber alignment. Compared to the EAN model group, both H-GG and L-GG treatments demonstrated improved axon organization and reduced demyelination (Fig. 1D).

GG Improves Peripheral Blood Immunological Dysbalance and Inhibits Inflammatory Factor Release in EAN.

EAN is characterized by elevated CD4+T cells and macrophages [16,17]. Therefore, we examined the immune balance using $CD4^+T/CD8^+T$ cell ratio post immunization on day 19. Peak disease stage revealed a $CD4^+T$ of 68.4 %, $CD8^+T$ of 27.5 % in the NC group; $CD4^+T$ of 82.4 %, $CD8^+T$ of 14.2 % in the EAN model group; $CD4^+T$ of 60.4 %, $CD8^+T$ of 35.5 % in the H-GG treatment group; and $CD4^+T$ of 71.4 %, $CD8^+T$ of 26.3 % in the L-GG treatment group.This indicated that both H-GG and L-GG treatments improved the immune imbalance (Fig. 2A and B). Reduced $CD3^+T$ cells in the EAN group may be due to T cell migration into peripheral nerve tissue during inflammation.Blood serum analysis of IL-1β and TNF-α levels at early and peak stages of the disease revealed significant upregulation in the EAN model group, but downregulation in the H-GG and L-GG treatment groups at peak stage (Fig. 2C), indicating that GG improves peripheral blood immunological dysbalance and inhibits inflammatory factor release in EAN.

3.2. GG significantly enhances gut barrier function and inhibits intestinal inflammation

As shown in Fig. 3A, EAN model gut mucosa exhibited structural disarray and tissue breach compared to H-GG or L-GG groups exhibiting normal mucosal architecture. qPCR of Occludin and ZO-1 genes at mRNA level demonstrated a notable decline in the EAN model, with an almost normalized expression in H-GG or L-GG groups (Fig. 3B). Notably, Reg3γ was upregulated in the EAN model but downregulated in both H-GG and L-GG groups (Fig. 3B). Furthermore, both H-GG and L-GG suppressed IL-1β and TNF-α expression during disease peak phase (Fig. 3C). These results underscore GG's potency in restoring gut barrier integrity and suppressing inflammation.

3.3. GG partially alleviates EAN-induced Disruption of gut microbiota

16S rRNA gene sequencing reveals significant increases in *Ruminococcaceae* (from 11.9 % to 24.2 %) and *Lachnospiracea* (from 3.1 % to 19.3 %) while reducing *Bacteroidaceae* (from 15.7 % to 9.6 %). H-GG treatment mitigated the EAN-induced increase in *Ruminococcaceae* (from 24.2 % to 16.8 %) and *Lachnospiracea* (from 19.3 % to 7.3 %), and boosted *Lactobacillus* family proportion (from 20.8 % to 28.2 %) (Fig. 4A). At genus level, the EAN model group upregulated *Ruminiclostridium 6*, *Ruminiclostridium 2*, *Oscillibacter, Ruminiclostridium 9*, and *Candidatus Soleaferrea* compared with the control group (Fig. 4B). However, H-GG downregulated expression of *Ruminiclostridium 2, Ruminiclostridium 6,* and Candidatus *Soleaferrea* induced by EAN (Fig. 4C).

3.4. GG partially improves metabolic imbalances in the gut

Metabolomics analysis on rat feces revealed a total of 1797 metabolites, with chemical classification revealing organic acids and their derivatives (23.205 %), lipids/lipoid molecules (21.48 %), and organic heterocyclic compounds (15.693 %) (Fig. 5A). The volcano plots for the EAN model group's unique metabolites compared to the NC group and H-GG group's unique metabolites compared to the EAN model group are shown in Fig. 5B and C respectively. The EAN model group exhibited 44 unique metabolites compared to the NC control group, with 19 upregulated and 25 downregulated (Fig. 6A). The H-GG treatment group showed 23 unique metabolites compared to the EAN model group, with 16 upregulated and 7 downregulated (Fig. 6B). Compared to control group, EAN upregulated Corticosterone, Trihydroxycholestanoic acid and Antheraxanthin, which were reversed by H-GG treatment; EAN downregulated L-Glutamate and Glutaric Acid, which were upregulated by H-GG treatment.

KEGG pathway analysis indicated that the EAN model group had upregulated pathways such as Protein digestion and absorption, Prion diseases, Biosynthesis of amino acids, Primary bile acid biosynthesis, but downregulated Neuroactive ligand-receptor interaction (Fig. 6C). In contrast, the H-GG group had upregulated pathways like Thiamine metabolism, Ferroptosis, Long-term potentiation, and downregulated pathways like Prion diseases, Primary bile acid biosynthesis (Fig. 6D).

4. Discussion

The human microbiome and metabolites are linked to immune-related neurological diseases [18,19]. In the EAN model, sterile mice show low proinflammatory cytokine production in intestines and spinal cords. Conversely, segmented filamentous bacteria exacerbate sterile mouse symptoms via Th1 and Th17 induction in the intestine and spinal cord [20], while *Bacteroides fragilis* ameliorates the disease through Treg cell promotion, suggesting an immune response modulatory role for gut microbes on inflammation [21]. Our findings suggest that GG mitigates EAN progression. We propose this is due to GG's ability to decrease IL-1β and TNF-α levels and regulate $CD4^+/CD8^+T$ cell balance. This aligns with prior studies demonstrating GG's immunomodulatory and anti-inflammatory properties [22,23].

Dysbiosis of the gut microbiota is a potential mechanism underlying autoimmune diseases (AIDs) [24]. Intestinal barrier integrity is crucial for maintaining microbial-host immune equilibrium, compromised host intestinal barriers lead to immune system hyperactivation [25]. However, AID patients often exhibit damaged and leaky gut walls [26], consistent with our results. In EAN, intestinal mucosal damage, elevated IL-1β and TNF-α, and reduced Occludin and ZO-1 expression occur. Occludin and ZO-1 are indicators of intestinal inflammation severity and mucosal healing prediction, with lower expression indicating more severe injury [27]. GG improves intestinal mucosal damage and inflammation by increasing ZO-1 and Occludin protein expression and reducing inflammatory factors. Additionally, Reg3γ, an inflammation-associated marker, shows increased expression with increased intestinal inflammation

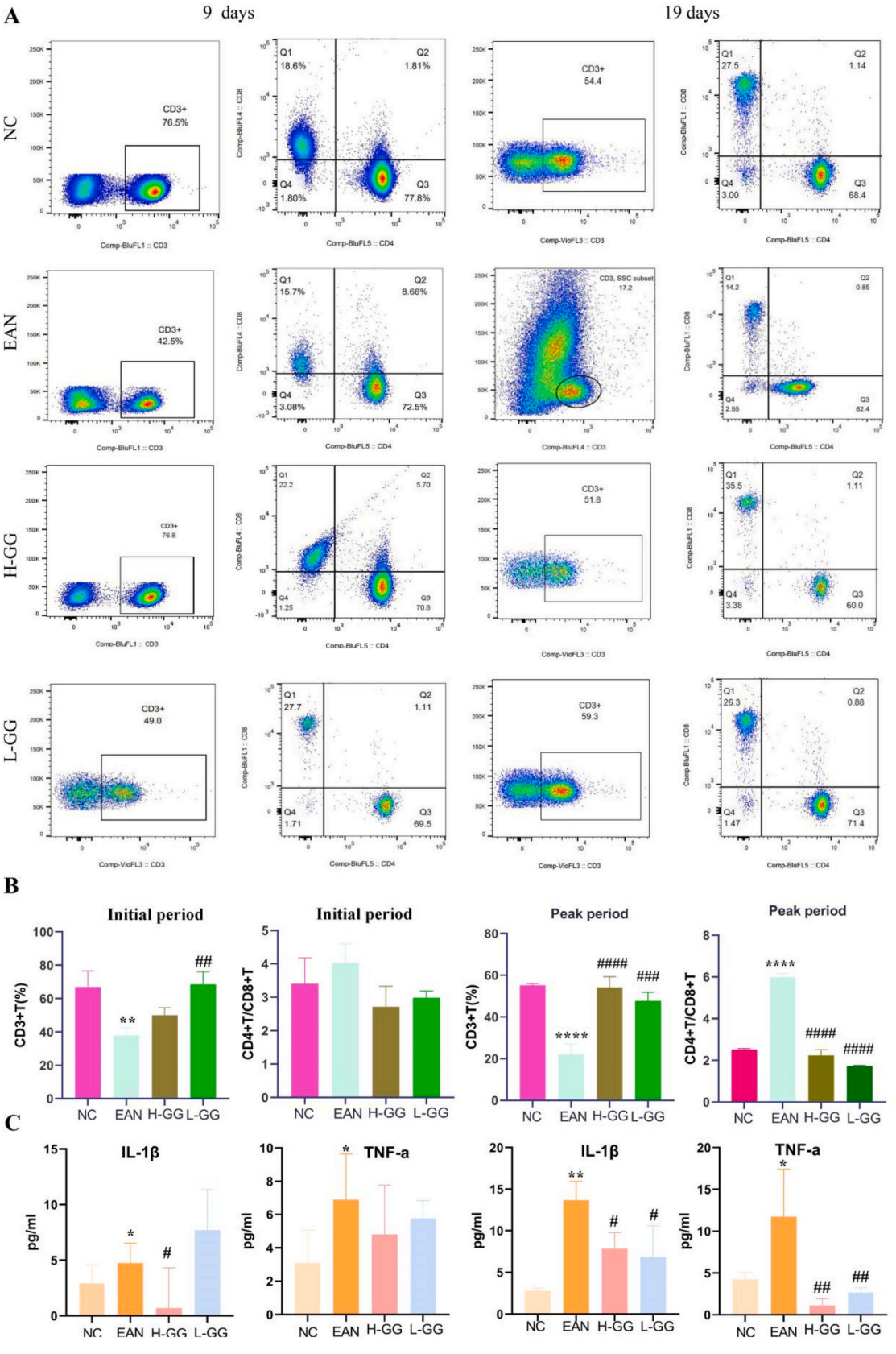

(caption on next page)

Fig. 2. GG improves peripheral blood immunological dysbalance and inhibits inflammatory factor release (n = 6). A, Flow cytometry analysis of peripheral blood T cells; B, Proportion of $CD3^{+}$T cells and $CD4^{+}/CD8^{+}$T cells in different treatment groups. C, Effect of H-GG and L-GG on the release of inflammatory factors IL-1βand TNF-α. (*$p < 0.05$, **$p < 0.01$, ****$p < 0.0001$, #$p < 0.05$, ##$p < 0.01$, ###$p < 0.001$, ####$p < 0.0001$).

[28]. Impaired intestinal barriers enhance gut microbe transfer, leading to abnormal contact between gut microbes and the host immune system, triggering autoimmunity through various mechanisms.

As research into the gut microbiota progresses, significant differences have been observed between the gut microbiota of AID patients and healthy individuals [29,30]. Specific bacterial strains can drive body-specific autoantibody production and immune activation, stimulating Th17 cell activation [31]. In our study, GG treatment resulted in a community structure closer to normal controls, whereas the EAN model group experienced changes, potentially related to GG's capacity to maintain immune equilibrium. However, the biological significance of microbiota shifts remains unclear and may be related to metabolic profile alterations. Therefore, we focused on gut metabolic profile alterations in further study.

Emerging evidence suggests that aberrant metabolites in AID promotes inflammatory cellular and molecular processes [32]. Compared to the control group, EAN upregulated Corticosterone, Trihydroxycholestanoic acid, and Antheraxanthin, which were reversed by GG treatment. Corticosterone is a potent anti-inflammatory hormone, however, exacerbated functional impairments in stressed EAE mice were highly correlated with circulating corticosterone levels [33]. Research indicates excessive

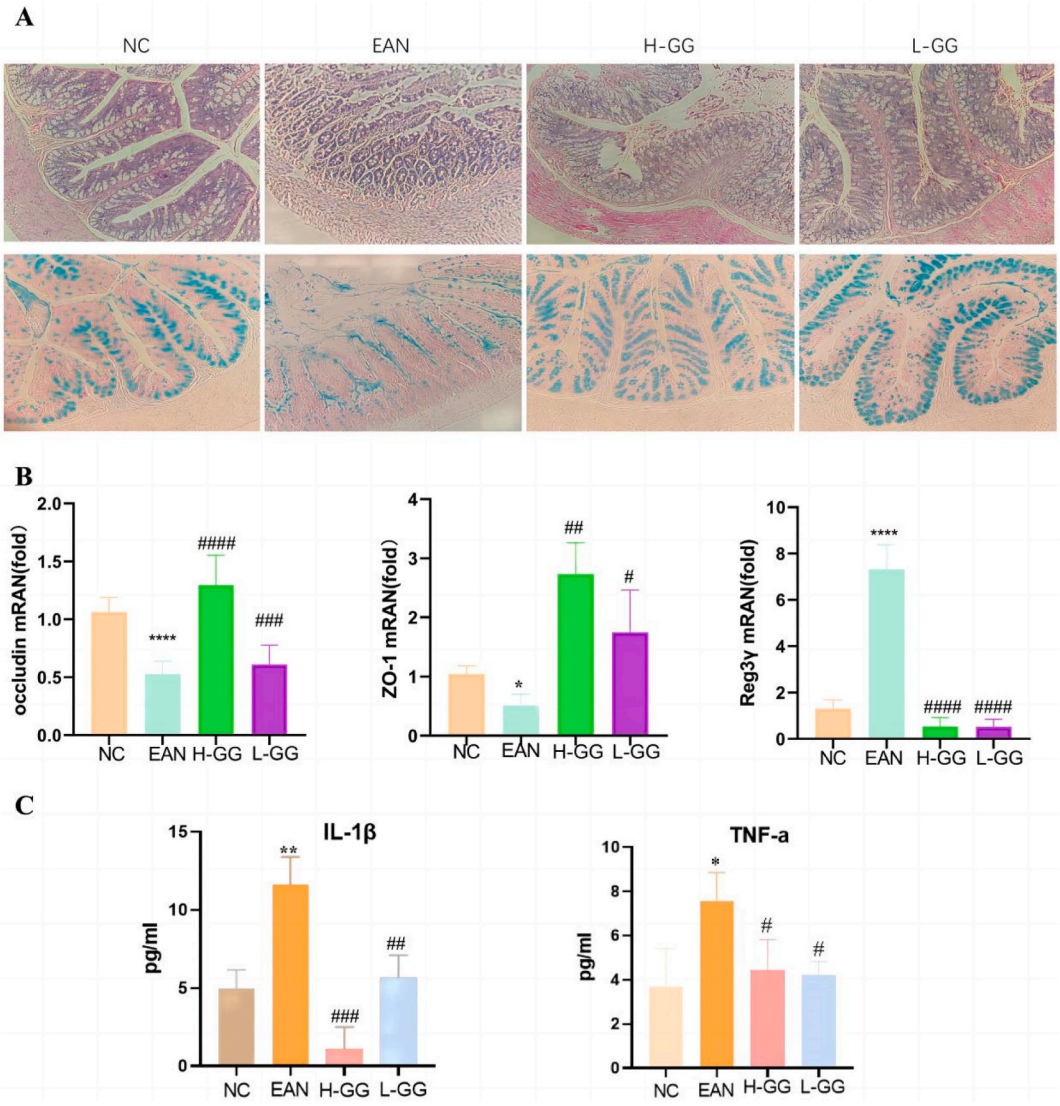

Fig. 3. GG significantly improves gut barrier function and inhibits intestinal inflammation (n = 6). A, Alcian blue staining of gut mucosa. B, Real-time PCR analysis of Occludin, ZO- 1, reg3γon day 19 post-immunization. C, ELISA detection of IL-1β and TNF-αexpression on day 19 post-immunization. (*$p < 0.05$, **$p < 0.01$, ****$p < 0.0001$, #$p < 0.05$, ##$p < 0.01$, ###$p < 0.001$, ####$p < 0.0001$).

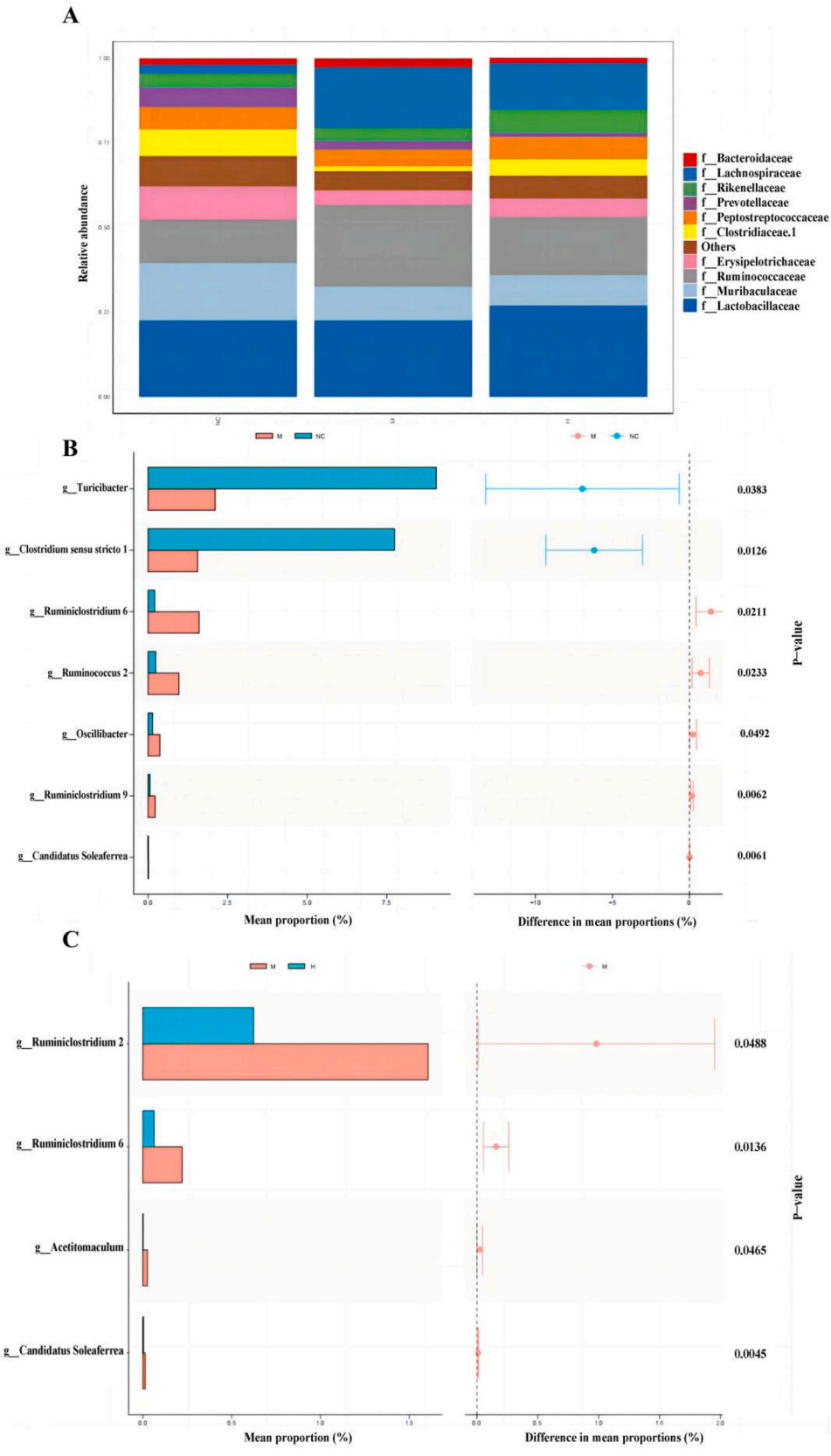

(caption on next page)

Fig. 4. GG Partially Alleviates Gut Microbiota Disruption Caused by EAN. A, Composition of microbiota at family level for each treatment group; B, Differential microbiota between the EAN model group and normal control group; C, Differential microbiota between the H-GG treatment group and EAN model group.

Trihydroxycholestanoic acid impairs peroxisomal function [34]. However, GG can alleviate excessive Inflammatory Response. EAN downregulated L-Glutamate and Glutaric Acid, which were upregulated by GG treatment. L-Glutamate, a nonessential amino acid, plays a pivotal role in the metabolism of CNS cells. It regulates the production of glutamate-derived neurotransmitters through tight

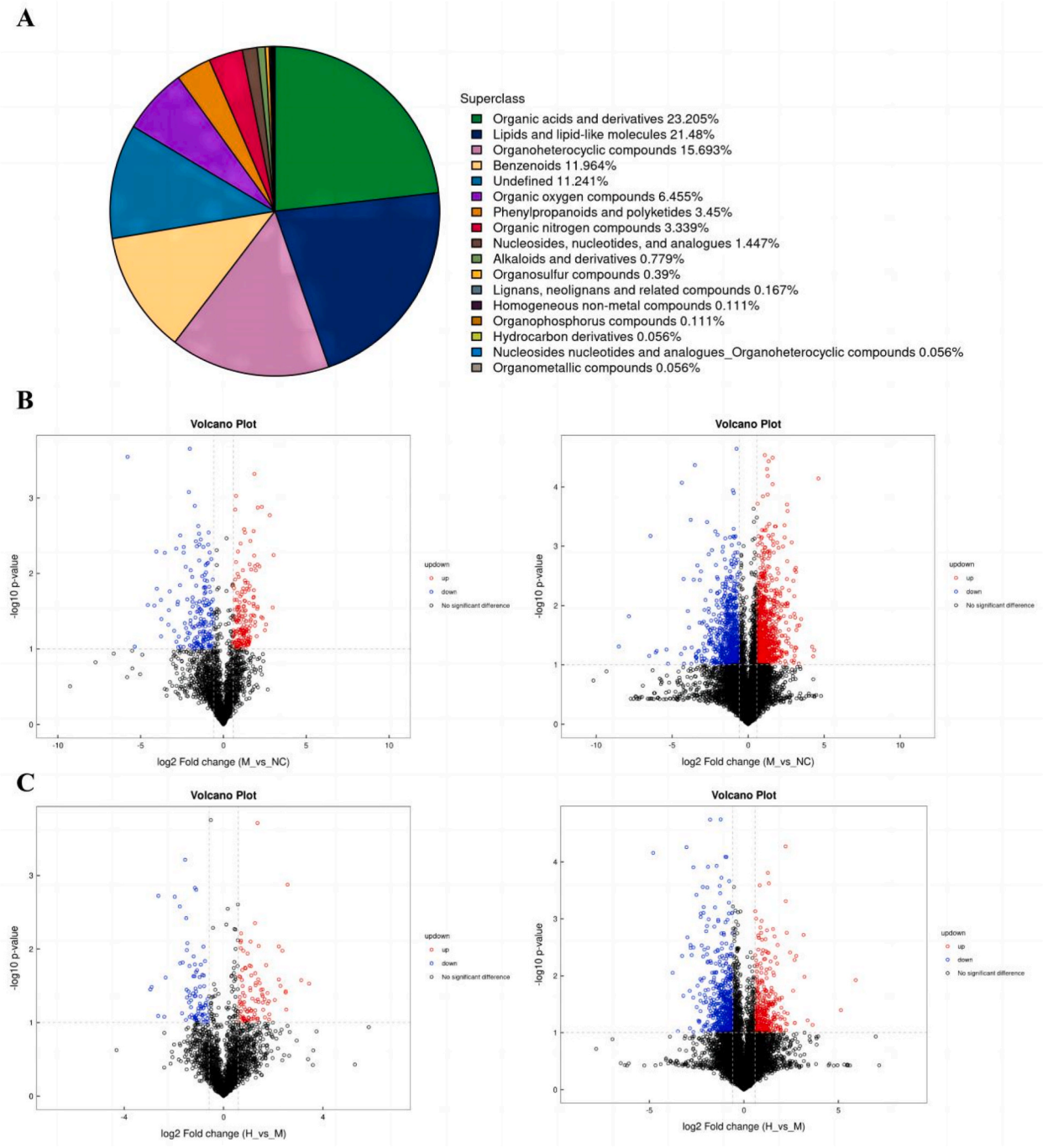

Fig. 5. Gut Microbial Differential Metabolites. A, Chemical classification of gut metabolites; B, Volcano plots (negative and positive) comparing EAN model group to NC group; C, Volcano plots (negative and positive) contrasting H-GG group with the EAN model group.

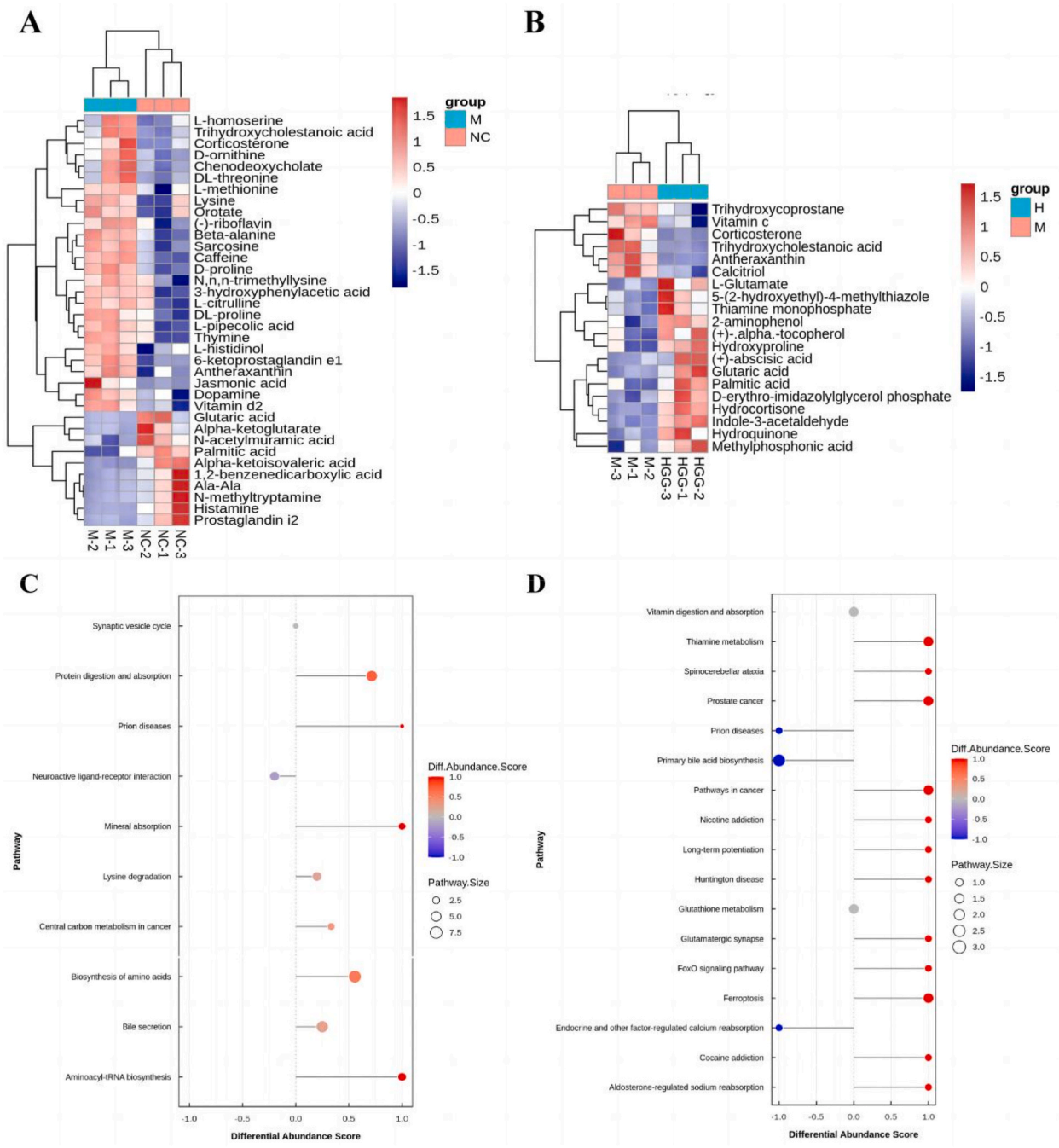

Fig. 6. Analysis of Gut Microbial Differential Metabolites and KEGG Pathways. A, Comparison of differential metabolites between EAN model group and NC group; B, Contrasting differential metabolites in H-GG group versus EAN model group; C, KEGG signaling pathway analysis of differential metabolites in EAN model group compared to normal control group; D, KEGG signaling pathway analysis of differential metabolites in H-GG treatment group versus EAN model group.

control of amino acid bioavailability in the neuron-astrocyte metabolic symbiosis. This system can be severely affected in disease states. L-glutamate converts glutamate into glutamine via glutaminase to decrease glutamate concentration. Additionally, L-glutamate can increase its concentration by transforming glutamate and ammonia into glutamine through glutamine synthase [35].These results also indicate that GG partially restores the composition of gut metabolites, thereby mitigating EAN progression.

5. Conclusion

GG effectively modulates the $CD4^+/CD8^+$ T cell ratio in EAN rat tail vein blood, reduces IL-1β and TNF-α expression, improves sciatic nerve demyelination and inflammation, and stimulates gut mucosal repair during disease progression. Post-GG treatment, the intestinal microbial architecture and metabolism of EAN model animals partially normalize. It is speculated that GG impacts the gut microbiome, altering microbiome- and metabolite profiles, thereby mitigating autoimmune neuropathies. This offers a novel therapeutic approach for this condition.

5.1. Ethical approval and consent to participate

All experimental protocols of this study were approved by the ethics committee of First Affiliated Hospital of Bengbu Medical College (the num ber: [2021]174). All methods were carried out in accordance with relevant guidelines and regulations. All methods are reported in accordance with ARRIVE guidelines (https://arriveguidelines.org) for the reporting of animal experiments.

CRediT authorship contribution statement

Peng Shi: Writing – original draft, Data curation. **Yu Li:** Data curation. **Hui Yang:** Data curation. **Qiang Li:** Validation, Formal analysis. **Qianqian Li:** Validation, Investigation. **Ming Ye:** Formal analysis. **Di Nian:** Writing – review & editing, Conceptualization.

6. Consent for publication

Not applicable.

7. Statement of data availability

The data are available from the corresponding author on reasonable request.

Funding

This work was supported by Anhui Provincial Key R&D Programmes (No: 20230429510702007 5)" and Natural Science Research Project of Anhui Educational Committee's Major Project (No. KJ2021ZD0084).

Declaration of competing interest

The authors declare that they have no known competing financial interests or personal relationships that could have appeared to influence the work reported in this paper.

Acknowledgements

Not applicable.

References

[1] P. Shang, M. Zhu, Y. Wang, et al., Axonal variants of Guillain-Barré syndrome: an update, J. Neurol. 268 (7) (2021) 2402–2419.
[2] L. Benedetti, Beronio A. BrianiC, et al., Increased incidence of axonal Guillain-Barré syndrome in La Spezia area of Italy: a 13-year follow-up study, J. Peripher. Nerv. Syst. 24 (1) (2019) 80–86.
[3] D. Shen, F. Chu, Y. Lang, et al., Beneficial or harmful role of macrophages in guillain-barré syndrome and experimental autoimmune neuritis, Mediat. Inflamm. 2018 (2018) 4286364.
[4] A.K. Jasti, C. Selmi, J.C. Sarmiento-Monroy, et al., Guillain-Barré syndrome: causes, immunopathogenic mechanisms and treatment, Expert Rev Clin Immu 12 (11) (2016) 1175–1189.
[5] H.L. Zhang, X.Y. Zheng, J. Zhu, Th1/Th2/Th17/Treg cytokines in Guillain-Barré syndrome and experimental autoimmune neuritis, Cytokine Growth F R. 24 (5) (2013) 443–453.
[6] P.T. Brooks, J.A. Bell, C.E. Bejcek, et al., An antibiotic depleted microbiome drives severe Campylobacter jejuni-mediated Type 1/17 colitis, Type 2 autoimmunity and neurologic sequelae in a mouse model, J. Neuroimmunol. 337 (2019) 577048.
[7] P.T. Brooks, K.A. Brakel, J.A. Bell, et al., Transplanted human fecal microbiota enhanced Guillain Barré syndrome autoantibody responses after Campylobacter jejuni infection in C57BL/6 mice, Microbiome 5 (1) (2017) 92.
[8] Y. Meng, X. Qiu, Z. Tang, et al., Lactobacillus paracasei L9 affects disease progression in experimental autoimmune neuritis by regulating intestinal flora structure and arginine metabolism, J. Neuroinflammation 20 (1) (2023) 122.
[9] N. Wilck, M.G. Matus, S.M. Kearney, et al., Salt-responsive gut commensal modulates T(H)17 axis and disease, Nature 551 (7682) (2017) 585–589.
[10] R.L. Fine, D.L. Mubiru, M.A. Kriegel, Friend or foe? Lactobacillus in the context of autoimmune disease, Adv. Immunol. 146 (2020) 29–56.
[11] Q. Mu, H. Zhang, X. Liao, et al., Control of lupus nephritis by changes of gut microbiota, Microbiome 5 (1) (2017) 73.
[12] D. Ríos-Covián, P. Ruas-Madiedo, MargollesA, et al., Intestinal short chain fatty acids and their link with diet and human health, Front. Microbiol. 7 (2016) 185.
[13] D.J. Morrison, T. Preston, Formation of short chain fatty acids by the gut microbiota and their impact on human metabolism, Gut Microb. 7 (3) (2016) 189–200.
[14] P.J. Brun, A. Grijalva, R. Rausch, et al., Retinoic acid receptor signaling is required to maintain glucose-stimulated insulin secretion and β-cell mass, FASEB J. 29 (2) (2015) 671–683.

[15] L. Cervantes-Barragan, J.N. Chai, M.D. Tianero, et al., Lactobacillus reuteri induces gut intraepithelial CD4(+)CD8αα(+) T cells, Science 357 (6353) (2017) 806–810.
[16] M. Yang, C. Peyret, X.Q. Shi, et al., Evidence from human and animal studies: pathological roles of CD8(+) T cells in autoimmune peripheral neuropathies, Front. Immunol. 6 (2015) 532.
[17] A.K. Mausberg, F. Szepanowski, F. Odoardi, et al., Trapped in the epineurium: early entry into the endoneurium is restricted toneuritogenic T cells in experimental autoimmune neuritis, J Neuroinflamm 15 (1) (2018) 217.
[18] Lung-brain axis, O. Bajinka, L. Simbilyabo, et al., Crit rev microbiol 48 (3) (2022) 257–269.
[19] O. Bajinka, Z. Tang, Y. Mao, et al., Respiratory syncytial virus infection disrupts pulmonary microbiota to induce microglia phenotype shift, J. Med. Virol. 95 (8) (2023) e28976.
[20] Y.K. Lee, J.S. Menezes, Y. Umesaki, et al., Proinflammatory T-cell responses to gut microbiota promote experimental autoimmune encephalomyelitis, Proc. Natl. Acad. Sci. USA 108 (Suppl 1) (2011) 4615–4622.
[21] A. Mangalam, S.K. Shahi, D. Luckey, et al., Human gut-derived commensal bacteria suppress CNS inflammatory and demyelinating disease, Cell Rep. 20 (6) (2017) 1269–1277.
[22] W.K. Kim, Y.J. Jang, D.H. Han, et al., Lactobacillus paracasei KBL382 administration attenuates atopic dermatitis by modulating immune response and gut microbiota, Gut Microb. 12 (1) (2020) 1–14.
[23] F. Wu, B. Fang, G. Wuri, et al., Metagenomic analysis reveals a mitigating role for lactobacillus paracasei and bifidobacterium animalis in experimental periodontitis, Nutrients 14 (10) (2022) 2125.
[24] G.L.V. De Oliveira, A.Z. Leite, B.S. Higuchi, et al., Intestinal dysbiosis and probiotic applications in autoimmune diseases, Immunology 152 (1) (2017) 1–12.
[25] O. Bajinka, Y. Tan, K.A. Abdelhalim, et al., Extrinsic factors influencing gut microbes, the immediate consequences and restoring eubiosis, Amb. Express 10 (1) (2020) 130.
[26] Y. Kinashi, K. Hase, Partners in leaky gut syndrome: intestinal dysbiosis and autoimmunity, Front. Immunol. 12 (2021) 673708.
[27] W.T. Kuo, L. Zuo, M.A. Odenwald, et al., The tight junction protein ZO- 1 is dispensable for barrier function but critical for effective mucosal repair, Gastroenterology 161 (6) (2021) 1924–1939.
[28] V.T.K. Le-Trilling, J.F. Ebel, F. Baier, et al., Acute cytomegalovirus infection modulates the intestinal microbiota and targets intestinal epithelial cells, Eur. J. Immunol. 53 (2) (2023) e2249940.
[29] X. Zhang, B.D. Chen, L.D. Zhao, et al., The gut microbiota: emerging evidence in autoimmune diseases, Trends Mol. Med. 26 (9) (2020) 862–873.
[30] Y. He, W. Wu, H.M. Zheng, et al., Regional variation limits applications of healthy gut microbiome reference ranges and disease models, Nat Med 24 (10) (2018) 1532–1535.
[31] M.E. Chriswell, Clay MR. LeffertsAR, et al., Clonal IgA and IgG autoantibodies from individuals at risk for rheumatoid arthritis identify an arthritogenic strain of Subdoligranulum, Sci. Transl. Med. 14 (668) (2022) eabn5166.
[32] B. Wu, T.V. Zhao, K. Jin, et al., Mitochondrial aspartate regulates TNF biogenesis and autoimmune tissue inflammation, Nat. Immunol. 22 (12) (2021) 1551–1562.
[33] J. Faraji, D. Bettenson, V.W. Yong, G.A.S. Metz, Early life stress aggravates disease pathogenesis in mice with experimental autoimmune encephalomyelitis: support for a two-hit hypothesis of multiple sclerosis etiology, J. Neuroimmunol. 385 (2023) 578240.
[34] R.J.A. Wanders, F.M. Vaz, H.R. Waterham, S. Ferdinandusse, Fatty acid oxidation in peroxisomes: enzymology, metabolic crosstalk with other organelles and peroxisomal disorders, Adv. Exp. Med. Biol. 1299 (2020) 55–70.
[35] F. Martins, L.G. Gonçalves, M. Pojo, J. Serpa, Take advantage of glutamine anaplerosis, the kernel of the metabolic rewiring in malignant gliomas, Biomolecules 10 (10) (2020) 1370.